A gating charge interaction required for late slow inactivation of the bacterial sodium channel NavAb

Tamer M. Gamal El-Din, Gilbert Q. Martinez, Jian Payandeh, Todd Scheuer, and William A. Catterall

Department of Pharmacology, University of Washington, Seattle, WA 98195

Voltage-gated sodium channels undergo slow inactivation during repetitive depolarizations, which controls the frequency and duration of bursts of action potentials and prevents excitotoxic cell death. Although homotetrameric bacterial sodium channels lack the intracellular linker-connecting homologous domains III and IV that causes fast inactivation of eukaryotic sodium channels, they retain the molecular mechanism for slow inactivation. Here, we examine the functional properties and slow inactivation of the bacterial sodium channel NavAb expressed in insect cells under conditions used for structural studies. NavAb activates at very negative membrane potentials ($V_{1/2}$ of approximately −98 mV), and it has both an early phase of slow inactivation that arises during single depolarizations and reverses rapidly, and a late use-dependent phase of slow inactivation that reverses very slowly. Mutation of Asn49 to Lys in the S2 segment in the extracellular negative cluster of the voltage sensor shifts the activation curve ∼75 mV to more positive potentials and abolishes the late phase of slow inactivation. The gating charge R3 interacts with Asn49 in the crystal structure of NavAb, and mutation of this residue to Cys causes a similar positive shift in the voltage dependence of activation and block of the late phase of slow inactivation as mutation N49K. Prolonged depolarizations that induce slow inactivation also cause hysteresis of gating charge movement, which results in a requirement for very negative membrane potentials to return gating charges to their resting state. Unexpectedly, the mutation N49K does not alter hysteresis of gating charge movement, even though it prevents the late phase of slow inactivation. Our results reveal an important molecular interaction between R3 in S4 and Asn49 in S2 that is crucial for voltage-dependent activation and for late slow inactivation of NavAb, and they introduce a NavAb mutant that enables detailed functional studies in parallel with structural analysis.

The Journal of General Physiology

INTRODUCTION

Voltage-gated sodium channels initiate action potentials in excitable cells. Neural signals are frequency modulated, and key information is encoded in the frequency of action potentials during bursts and in the duration and pattern of bursts. The action potential firing properties of neurons depend on the availability of sodium channels in the resting state. Two molecular mechanisms with strikingly different time scales are responsible for inactivating eukaryotic voltage-gated sodium channels: fast inactivation on the millisecond time scale (Hodgkin and Huxley, 1952; Catterall, 2000; Ulbricht, 2005) and slow inactivation on the time scale of hundreds of milliseconds to seconds (Rudy, 1978; Vilin and Ruben, 2001; Ulbricht, 2005). Fast inactivation of eukaryotic sodium channels occurs via the linker connecting domains III and IV, which folds into the intracellular mouth of the pore and blocks it like a hinged lid (Vassilev et al., 1988; Catterall, 2000). The mechanism of voltage-dependent slow inactivation involves structural changes in the selectivity filter and the pore-lining S6 segments (Ruff et al., 1987; Ruben et al., 1990; Kühn and Greeff, 1999; Vilin and Ruben, 2001; Vilin et al., 2001; Chen et al., 2006). The S4 segment has a crucial role in coupling activation to inactivation (Chen et al., 1996; Cha et al., 1999). Bacterial sodium channels are homotetramers of identical subunits (Ren et al., 2001). They lack the linker between domains III and IV, which is required for fast inactivation of eukaryotic sodium channels, but they retain a slow-inactivation process (Pavlov et al., 2005). Each subunit has the structure of one domain of a eukaryotic sodium channel, with six transmembrane segments (S1–S6) that form a voltage-sensing module (S1–S4) and a pore module (S5–S6 and the intervening P loop) (Ren et al., 2001; Payandeh et al., 2011). The crystal structure of NavAb from the Gram-negative bacterium *Arcobacter butzleri* has been solved at high resolution, revealing the three-dimensional organization of these functional modules (Payandeh et al., 2011). When NavAb WT is expressed in insect cells, it activates at very negative potentials (V_a of approximately −98 mV) and shows strongly use-dependent inactivation that hinders electrophysiological studies (Payandeh et al., 2012). To define the inactivation

Correspondence to William A. Catterall: wcatt@uw.edu

J. Payandeh's present address is Dept. of Structural Biology, Genentech Inc., South San Francisco, CA 94080.

Abbreviation used in this paper: HP, holding potential.

The Rockefeller University Press $30.00
J. Gen. Physiol. Vol. 142 No. 3 181–190
www.jgp.org/cgi/doi/10.1085/jgp.201311012

properties of NavAb at the molecular level, we sought single–amino acid mutations that would shift its activation into a more positive voltage range, prevent its late use-dependent slow inactivation, and thereby allow more detailed study of the three phases of slow inactivation. The S4 gating charges of NavAb interact with a cluster of fully or partially negatively charged residues at the outer ends of the S1 and S2 segments (Payandeh et al., 2011, 2012). In light of previous studies showing that the highly conserved gating charge–interacting residue at the extracellular end of the S2 segment (Asn49 in NavAb) is important in controlling the voltage dependence of activation (Zhao et al., 2004a; Blanchet et al., 2007), we mutated Asn49 to positively charged Lys (N49K) and analyzed the function of this mutant. To our surprise, this mutation not only greatly shifted the voltage dependence of NavAb activation to more positive membrane potentials but also abolished the late use-dependent phase of slow inactivation. Here, we present the biophysical properties of NavAb/N49K and suggest the hypothesis that interaction of the R3 gating charge in the S4 segment with N49 or its equivalent is required for normal activation of the voltage sensor and coupling to slow inactivation. Block of the late slow-inactivation process of NavAb with the N49K mutation also opens the way for detailed studies of its other biophysical properties.

MATERIALS AND METHODS

Mutagenesis and expression in insect cells

NavAb was cloned from *A. butzleri* (Payandeh et al., 2011). All mutants in this study were made in NavAb WT channel, except as explicitly noted for NavAb-I217C/R3C, in a modified p-FastBac Dual expression vector (Invitrogen), which is suitable for insect cells. Single-point mutations were introduced using PCR (QuikChange; Agilent Technologies). All mutants were verified by sequencing the mutated cDNA. NavAb WT and mutant constructs were expressed in *Trichopulsia ni* insect cells (High Five; Invitrogen) using recombinant baculovirus generated using the Bac-to-Bac system (Invitrogen). Cells were grown on 35-mm Petri dishes. They were incubated in Grace's insect medium (Gibco) supplemented with FBS (10%) and antibiotics (100 µg/ml streptomycin and 100 U/ml penicillin). Cells were infected by replacing the incubation medium with a medium containing the virus encoding the WT or mutant channel (10 µg/ml). After 1 h, 2 ml of incubation medium was added to the virus-containing medium. Cells were maintained at 25–27°C for at least 24 h before study.

Electrophysiology

All constructs showed high level expression that enabled us to measure ionic current and gating currents 24–48 h after infection. Whole-cell sodium currents were recorded using an amplifier (Axopatch 200; Molecular Devices) with glass micropipettes (2–5 MΩ). Capacitance was subtracted and series resistance was compensated using internal amplifier circuitry; 80–85% of series resistance was compensated. For ionic current measurements, the intracellular pipette solution contained (mM): 35 NaCl, 105 CsF, 10 EGTA, and 10 HEPES, pH 7.4 (adjusted with CsOH). The extracellular solution contained (mM): 140 NaCl, 2 $CaCl_2$, 2 $MgCl_2$, and 10 HEPES, pH 7.4 (adjusted with NaOH). For gating current measurements, the intracellular pipette solution contained (mM): 140 NMDG-F, 5 mM choline-Cl, 10 mM HEPES-NMDG, and 10 mM EGTA-NMDG, pH 7.4 (adjusted with H_2SO_4). The extracellular solution contained (mM): 140 NMDG-$MeSO_3$ and 10 HEPES-NMDG, pH 7.4 (adjusted with H_2SO_4). For NavAb/N49K ionic current measurements, the standard clamp protocol consisted of steps from a holding potential (HP) of −120 mV to voltages ranging from −120 to +70 mV in 5-mV steps. For the R3C-I217C and R4C mutants, the same protocol was applied but in 10-mV steps. Gating currents were measured from two different HPs: −80 and 0 mV. For HP of −80 mV, cells were held at −80 mV for 2–3 min, and a short pulse (30 ms) to −160 mV was applied, followed by 20-ms pulses from −200 mV up to +60 mV in 10-mV steps. For 0-mV HP measurements, the cells were held at 0 mV for 2–3 min, and 20-ms hyperpolarizing pulses (0 to −200 mV) in 5-mV steps were applied. Voltage-clamp pulses were generated and currents were recorded using Pulse software controlling an Instrutech ITC18 interface (HEKA). Data were analyzed using Igor Pro 6.2 software (WaveMetrics).

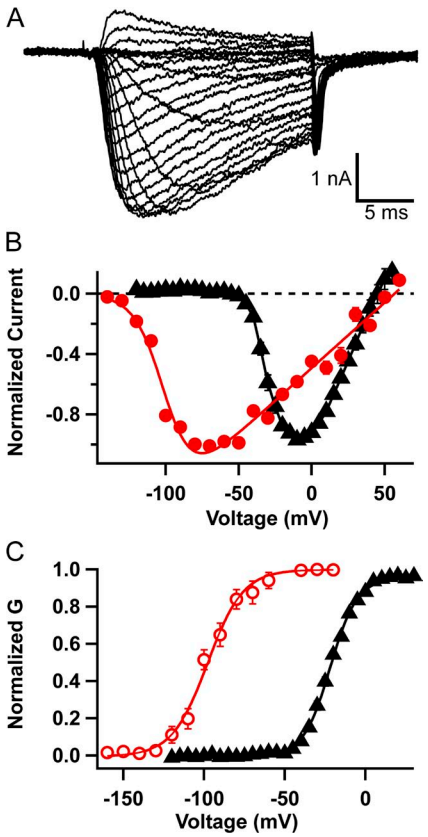

Figure 1. Comparison of NavAb/N49K and NavAb WT channels. (A) NavAb/N49K currents in response to depolarizations to potentials ranging from −55 to +60 mV in 5-mV increments. (B) Peak current–voltage relationships for NavAb WT (red circles) and NavAb/N49K (black triangles). (C) Conductance–voltage relationships for NavAb WT (red circles) and NavAb/N49K (black triangles). The lines through the curves are fits of Boltzmann relationships with values of V_a = −21.9 mV and k = 8.3 mV for NavAb N49K, and V_a = −97.8 mV and k = 11.0 mV for NavAb WT.

RESULTS

Mutation N49K causes a strong positive shift in the voltage dependence of activation

NavAb WT channels expressed in High Five insect cells activate at very negative potentials, with observable sodium currents at approximately −130 mV and peak current at approximately −75 mV (Fig. 1 B, red). The negative voltage dependence and strong use-dependent inactivation (Payandeh et al., 2012, and see below) make electrophysiological measurements of the biophysical properties of the channel challenging. We previously found that substituting the outer conserved negatively charged Asp in the S2 segment of the voltage sensor of NaChBac with Lys resulted in a +75-mV shift in the voltage dependence of activation (Zhao et al., 2004b). The amino acid in the analogous position of NavAb is Asn49. As in NaChBac, mutating NavAb Asn49 to a Lys, N49K, resulted in a +76-mV shift in the current–voltage relationship (Fig. 1, A and B, black) and the voltage dependence of activation (Fig. 1 C; NavAb WT, half-activation voltage, $V_a = -97.8 \pm 1.2$ mV; NavAb/N49K, $V_a = -21.9 \pm 0.3$ mV). Insertion of Lys at this key position in NavAb strongly favors the deactivated state of the voltage sensor relative to the activated state.

Late slow inactivation of WT NavAb is absent in NavAb/N49K

NavAb WT is characterized by a striking, slowly reversible form of use-dependent inactivation (Payandeh et al., 2012). Repetitive depolarizations to −10 mV from an HP of −180 mV at a frequency of 0.2 Hz resulted in reduction of current amplitude to ∼25% of its initial value after 20 pulses (Fig. 2, A and B, red traces and symbols). Surprisingly, the same protocol produced almost no decline in current conducted by NavAb/N49K (Fig. 2, A and B, black traces and symbols). Moreover, repetitive pulses to a more depolarized potential, +70 mV, for 200 s reduced the current <10% (Fig. 2, A and B, blue traces and symbols). Thus, mutation N49K prevented this striking form of late slow inactivation in addition to its effects on voltage-dependent activation.

Inactivation properties of NavAb/N49K

Despite lacking the late use-dependent, slow-inactivation process, NavAb/N49K channels still inactivate during short depolarizing pulses, with a time constant that reaches a limiting value of ∼21 ms for potentials positive to +30 mV (Fig. 3 A). This is significantly slower than NavAb WT, which reaches a plateau of ∼11 ms at positive potentials (Fig. 3 A; Payandeh et al., 2012). The voltage dependence of inactivation of NavAb/N49K studied with 100-ms conditioning prepulses was shifted ∼60 mV toward more positive potentials. (Fig. 3 B; NavAb WT, $V_{1/2} = -119.3 \pm 0.8$ mV; NavAb/N49K, $V_{1/2} = -59.3 \pm 0.7$ mV). This positive shift in the voltage dependence of inactivation resembles the corresponding shift in the activation properties of mutant NavAb/N49K, but the magnitude of the shift is 16 mV less.

NavAb WT recovers from inactivation with multiple exponential components (Payandeh et al., 2012). Recovery

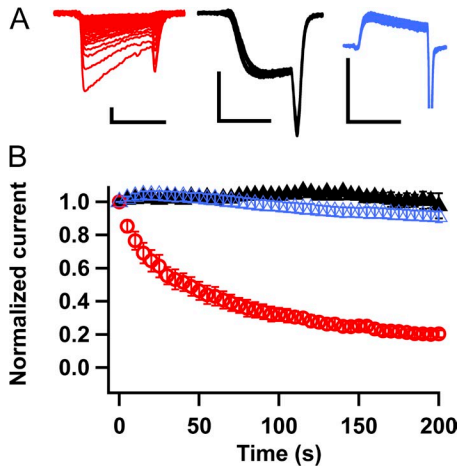

Figure 2. Loss of persistent inactivation in NavAb/N49K. (A) Current traces in response to repetitive 7-ms depolarizations to −10 mV applied at 0.2 Hz in NavAb WT (red traces; largest trace was produced by the first depolarization). Current traces elicited by 7-ms depolarization to −10 mV (black) and +70 mV (blue) for NavAb/N49K. Bars: vertical, 2 nA; horizontal, 5 ms. (B) Normalized peak inward currents measured during each pulse of trains and normalized to the current produced by the first depolarization of the train in NavAb WT (red circles) and NavAb/N49K (black and blue triangles).

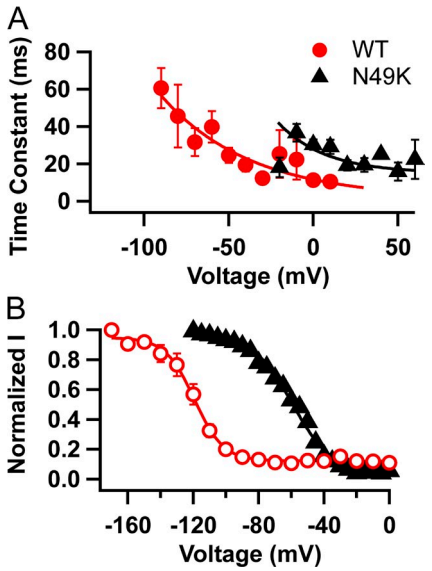

Figure 3. Comparison of inactivation properties of NavAb WT and NavAb/N49K. (A) Time constant of the decay of current during depolarizations to the indicated potentials for NavAb WT (red circles) and NavAb/N49K (black triangles). (B) Voltage dependence of inactivation for NavAb WT (red circles) and NavAb/N49K (black triangles) by depolarizations to −10 mV after 100-ms long conditioning prepulses to the indicated potentials.

after a 100-ms depolarizing prepulse followed a double-exponential time course, with mean time constants of 101 ms representing 77% of the recovering current and 3.2 s representing 23% of the recovering current; 8% of the sodium current failed to recover in the time allotted (20 s). These values yielded a weighted time constant of 819 ms (Fig. 4 A, red). Recovery from inactivation of NavAb/N49K at −120 mV after a 2.5-s depolarization was characterized by a double-exponential time course, with a fast time constant of ∼73 ms and a slow one of ∼727 ms. Recovery from inactivation after a 4-s prepulse (Fig. 4 A, black) was also biexponential, with a fast time constant of 47.6 ms representing 68% of the current and a slow time constant of 320 ms representing 32% of the current. Extending the prepulse to 10 s resulted in 62% of the current recovering with a time constant of 62 ms and 38% recovering with a time constant of 561 ms; 12% of the current failed to recover in the time allotted (Fig. 4 B). These values represent a weighted time constant of 250 ms. Even after this 100-fold longer prepulse, NavAb/N49K recovers from inactivation approximately three times faster than NavAb/WT. In addition, the slowest component of recovery is still 5.7-fold faster for NavAb/N49K. The slowly recovering component of inactivation is far less stable in NavAb/N49K than in NavAb/WT. In addition, this slowly recovering component of inactivation in NavAb/WT is induced within 100 ms but requires far longer depolarizations to be observed in NavAb/N49K.

The degree to which the slowly recovering component of inactivation has been abolished in NavAb/N49K is highlighted by the lack of effect of prolonged depolarizations to 0 mV. During repetitive 200-ms pulses to 10 mV applied at 0.2 Hz from an HP of −120 mV, current traces superimpose even though current inactivates virtually completely during each 200-ms test pulse (Fig. 4 C). Thus, recovery from inactivation is virtually complete during the 4.8 s between depolarizations. To further examine the resistance to persistent inactivation, the membrane potential was changed to 0 mV for 2 min (Fig. 4 C). After these prolonged depolarizations, the membrane potential was returned to −120 mV, and the 0.2-Hz pulse protocol was resumed. The first pulse initiated immediately upon returning to −120 mV showed no current because of inactivation during the preceding depolarization; the second one applied 5 s after repolarization showed complete recovery of current to its original amplitude. Experiments with depolarizations ranging from 1 to 5 min gave similar results. No prolonged component of inactivation with slow recovery was produced, confirming that N49K mutation abolishes the late slow inactivation that is so prominent in the NavAb WT channel.

Gating currents of NavAb/N49K

In most voltage-gated channels, gating charge movement is altered in parallel with the slow-inactivation process (Bezanilla et al., 1982; Olcese et al., 1997). We measured gating charge movement in Na_VAb/N49K using an HP of −80 mV followed by a 20-ms prepulse to −160 mV before steps to different test potentials (Fig. 5 A, blue). The time integral of the ON I_g showed that, with

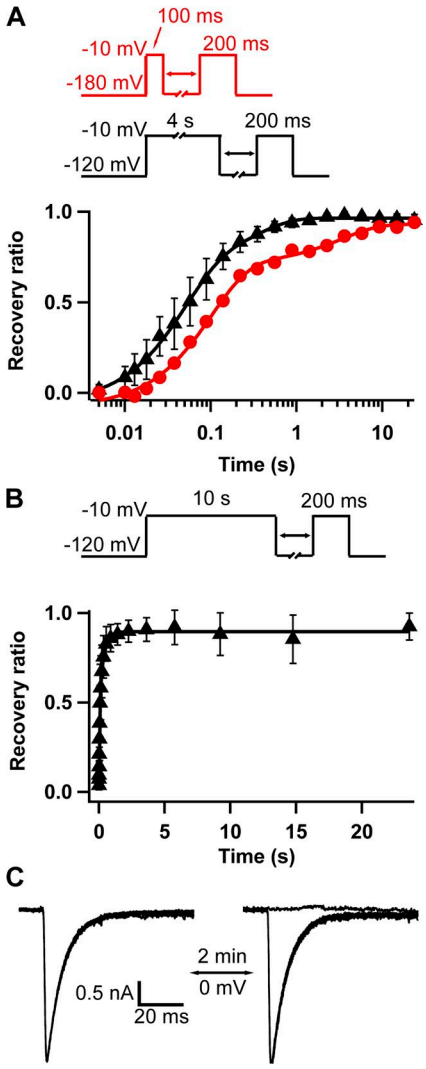

Figure 4. Comparison of recovery from inactivation for NavAb WT and NavAb/N49K. (A) Recovery from inactivation for NavAb WT studied with a 100-ms pre-depolarization (red protocol and circles) and for NavAb/N49K studied with a 4-s pre-depolarization (black protocol and triangles). Pre-depolarizations to induce inactivation were followed after a variable recovery interval by a test depolarization to −10 mV. Peak current measured during the test depolarization was normalized to the peak current during the pre-depolarization and plotted as a function of the recovery interval. (B) Recovery from inactivation for NavAb/N49K studied as described above but using a 10-s pre-depolarization to induce inactivation. (C) Eight superimposed depolarizations to 0 mV for NavAb/N49K applied at 0.2 Hz from an HP of −120 mV (left-hand traces) were followed by a 2-min maintained depolarization to 0 mV. The membrane potential was then returned to −120 mV, and the 0.2-Hz train of depolarizations to 0 mV was resumed (right-hand traces). The first depolarization, applied 10 ms after returning to −120 mV, resulted in the trace with no inward current. Current traces elicited by nine additional subsequent depolarizations are shown superimposed.

an HP of −80 mV, gating charge movement was first observed during depolarizations to approximately −130 mV and was described by a sigmoidal voltage dependence with a midpoint of −58.4 ± 1.9 mV (n = 5) (Fig. 5, B and C, blue). Thus, gating charge movement is characterized by a voltage dependence that is 36 mV more negative than the voltage dependence of channel opening (Fig. 5 C, black; V_a of approximately −50 mV), and nearly all gating charge has moved outward before activation of the ionic current is detectable. For some voltage-gated channels, the voltage dependence of gating charge movement is strongly shifted to negative potentials during prolonged depolarization, in parallel with the development of slow inactivation (Bezanilla et al., 1982; Olcese et al., 1997). Because NavAb/N49K lacked the late phase of slow inactivation, we examined whether it also lacked the hysteresis of gating charge movement induced by prolonged depolarization. To study the hysteresis of the QV curve, cells were held at 0 mV, and charge movement was measured in response to hyperpolarizations from this potential. The QV curve shows that the gating charge moves between approximately −80 mV and approximately −170 mV with a midpoint of −133.6 ± 1.01 mV (n = 7) (Fig. 5 C, green). The striking −76-mV shift in midpoint relative to the results with an HP of −80 mV (Fig. 5, B and C, blue) indicates that mutant N49K has retained gating charge hysteresis, despite having profoundly altered slow inactivation. To be sure that the same charge was moving from the two HPs and only its voltage dependence was changed, we compared the absolute amount of gating charge that moves during depolarizations of a single cell from −160 mV to the amount of gating charge that moves during hyperpolarizations from an HP of 0 mV (Fig. 5 D). The results show that the total amount of charge that moves is the same using the two different HPs, despite the large difference in the voltage dependence of gating charge movement. We also compared ON and OFF gating charge movement at each HP to detect any immobilization of charge that occurred during short depolarizing pulses. For depolarizations from −160 mV, the gating charge that was transferred during depolarization returned with the same voltage dependence upon hyperpolarization (Fig. 5 E). Likewise, in experiments using

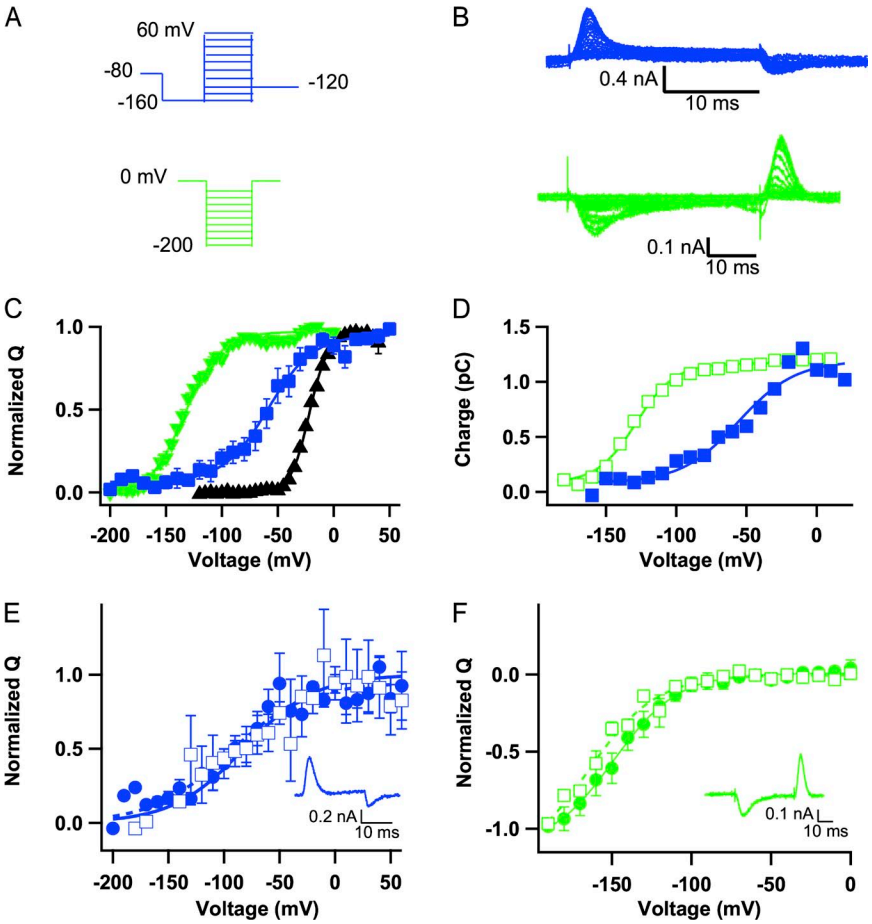

Figure 5. Properties of NavAb/N49K gating currents. (A) Protocols for measuring gating currents measured using HPs of −80 mV (blue) or 0 mV (green). When the HP was −80 mV, gating currents were measured after prepulse to −160 mV for 20 ms, followed by depolarizations to the indicated potentials. Subtraction of linear currents was by P/4 using an HP of 0 mV. When the HP was 0 mV, gating currents were measured in response to hyperpolarizing steps to a range of more hyperpolarized potentials. (B) Examples of gating current traces obtained from an HP of −80 mV (blue) or 0 mV (green). (C) Mean voltage dependence of gating current obtained using the −80-mV (blue squares) or 0-mV (green inverted triangles) HPs. The lines through the values are Boltzmann fits with the following values: HP of −80 mV (blue), half-activation potential (V_g) = −58.4 mV and slope (k) = 20 mV; HP of 0 mV (green), V_g = −133.6 mV and k = 16.4 mV. The conductance–voltage relationship from Fig. 1 C (black triangles and fit) is shown for comparison. (D) Measurements from a representative cell comparing the amount of charge measured using an HP of −80 mV (blue closed squares) and using an HP of 0 mV (green open squares). Charge measured in response to the depolarizing step was integrated in each case (beginning of pulse for HP of −80 mV; end of pulse for HP of 0 mV). (E) Q-V curves of ON charge movement in response to depolarization using an HP of −80 mV (blue closed circles) and OFF charge movement upon hyperpolarization (blue open squares). ON and OFF charge for each cell was normalized to the maximum ON charge for that cell. (F) Q-V curves of charge movement upon hyperpolarization (green open squares) and upon depolarization (green closed circles) measured using an HP of 0 mV.

an HP of 0 mV, charge that was transferred during hyperpolarizing steps returned with a similar voltage dependence upon repolarization (Fig. 5 F). Thus, gating charge is conserved for reciprocal voltage steps as expected if charge immobilization is minimal in this channel for these short-duration voltage excursions.

Interaction between arginine gating charges and Asn49

Asn49 and its analogue Asp60 in NaChBac contribute to the extracellular negative cluster and interact with the gating charges of the S4 segment, as observed in both disulfide-locking experiments and high resolution crystal structures (DeCaen et al., 2008, 2009; Payandeh et al., 2011, 2012). In addition, NaChBac channels in which covalent linkage between D60C and R3C has been induced by disulfide cross-linking open and then enter a slow-inactivated state (DeCaen et al., 2008, 2009). Therefore, we tested whether substitution of Cys for R3 in NavAb might mimic the effects of N49K. Unfortunately, NavAb/R3C, NavAb/R3G, and NavAb/R3Q did not produce measurable ionic or gating currents, even though the NavAb/R3C mutant protein was well expressed in insect cells, as assessed by fluorescence of an epitope tag and absorbance in size-exclusion chromatography of the isolated protein. Therefore, we introduced the R3C mutation into the genetic background of NavAb-I217C, which has less pronounced use-dependent inactivation at negative stimulus voltages than WT (Payandeh et al., 2012). NavAb-I217C activates at even more hyperpolarized potentials than NavAb WT does ($V_{1/2}$ = −123.9 mV for NavAb-I217C vs. −97.8 mV for NavAb WT). The voltage dependence of activation of NavAb/I217C-R3C was strongly shifted to positive membrane potentials (+102 mV; Fig. 6 A), resulting in similar voltage dependence of activation as N49K. These results suggest that these two mutations destabilize the open state to comparable extents and may act via the same mechanism.

The R4 gating charge also interacts with Asp60 in NaChBac during activation of the voltage sensor, as assessed by disulfide locking (DeCaen et al., 2009). Like R3C, mutation R4C inserted in the genetic background of NavAb WT also strongly shifted the voltage dependence of activation to more positive membrane potentials, but its shift of +43 mV (Fig. 6 B) was much less than for NavAb-I217C/R3C or NavAb/N49K. These results suggest that the native interactions of gating charge R4 substantially stabilize the activated state relative to the resting states in WT NavAb, similar to the native interactions of R3C with its ion pair and hydrogen bonding partners.

Despite the strong positive shifts in voltage-dependent gating induced by the mutations R3C and R4C, they had strikingly different effects on slow inactivation.

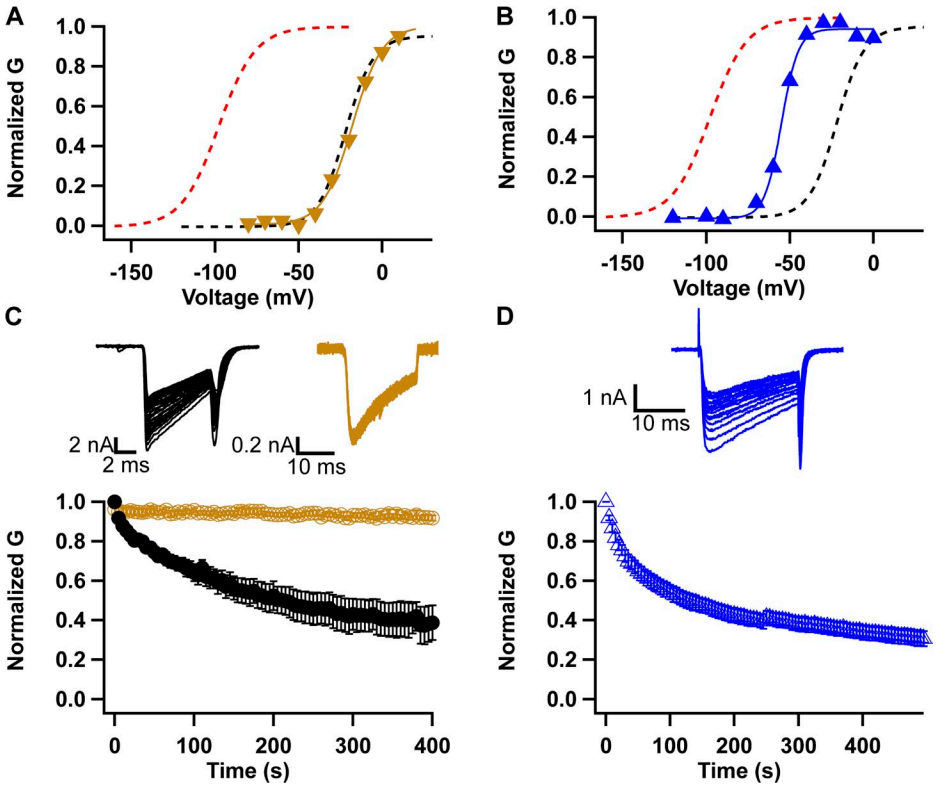

Figure 6. Characteristics of NavAb/R3C and NavAb/R4C. (A) Conductance–voltage relationship for activation of NavAb/I217C-R3C (gold inverted triangles). The line is a fit of a Boltzmann equation to the points, with V_a = −17.9 mV and k = 8.9 mV. The dotted lines are the fits to the conductance–voltage curves for NavAb WT (red) and NavAb/N49K (black) from Fig. 1 C. (B) Conductance–voltage relationship for activation of NavAb R4C (blue triangles). The line is a fit of a Boltzmann equation to the points, with V_a = −55.1 mV and k = 5.1 mV. Fit curves from Fig. 1 C for NavAb WT (red dashed line) and NavAb/N49K (black dashed line) are also shown for comparison. (C) Pulse-dependent inactivation of NavAb/I217C (black traces and symbols) and NavAb I217C/R3C (gold traces and symbols). Cells expressing NavAb/I217C and NavAb/I217C-R3C were subjected to depolarizations for 20 ms to either 0 mV (NavAb/I217C) or −10 mV (NavAb/I217C-R3C) at 0.75 Hz. Normalized peak inward current as a function of time is plotted. Traces 1–100 from example experiments are shown superimposed (insets). (D) Pulse-dependent inactivation of NavAb R4C. Cells expressing NavAb/R4C were subjected to depolarizations for 20 ms to −10 mV at 0.2 Hz. Normalized peak inward current as a function of time is plotted. Traces 1–18 from an example experiment are shown superimposed (inset).

NavAb/I217C-R3C had little or no late use-dependent slow inactivation, just as observed for NavAb/N49K (Fig. 6 C). In contrast, the strong use-dependent slow inactivation that is characteristic of NavAb WT was also observed for NavAb/R4C (Fig. 6 D). Thus, introduction of the mutation R3C produces a phenotype that is strikingly similar to that produced by N49K, but R4C does not, even though both cause strong positive shifts in the voltage dependence of activation.

DISCUSSION

Multiple phases of slow inactivation in NavAb

Our results presented previously (Payandeh et al., 2012) and here reveal three kinetic phases of inactivation in the bacterial sodium channel NavAb: two phases of reversible inactivation arising during single depolarizations, and a late phase of extremely slowly reversible inactivation that arises in repetitive pulsing and results in cumulative loss of sodium current. We use the term "slow inactivation" for all three phases of inactivation of NavAb, even though the early phases of slow inactivation arise relatively rapidly during single depolarizing pulses, because this form of inactivation is still 10-fold slower than fast inactivation of a eukaryotic sodium channel, and the structures required for the fast-inactivation process of eukaryotic sodium channels are missing in NavAb. In addition, NavAb inactivation shares an important mechanistic element with slow inactivation of eukaryotic sodium channels: striking hysteresis of gating charge movement that results in a requirement for very negative HPs for return of gating charge from the slow-activated state, as discussed below.

A molecular interaction required for late slow inactivation in NavAb

Our results show that the mutation N49K differentiates between two kinetic phases of slow inactivation. The two early, reversible phases of slow inactivation observed in single depolarizations are relatively unaffected by the N49K mutation. In sharp contrast, the late slowly reversible phase of slow inactivation is virtually completely blocked by the N49K mutation. Asn49 is in the position of a key gating charge–neutralizing residue in the extracellular negative cluster that is conserved in the S2 segments of all sodium channels (DeCaen et al., 2008, 2009; Payandeh et al., 2011). Therefore, it is likely that changing it from a hydrophilic, partially negatively charged residue to a positively charged one alters voltage-sensor function in a manner that prevents late slow inactivation. Consistent with the idea that interaction of Asn49 with gating charge R3 is crucial for slow inactivation, the effect of the mutation N49K in NavAb is mimicked by the mutation R3C in the S4 segment. Like N49K, this mutation spares the two early phases of inactivation that develop rapidly during single depolarizations. Thus, rapid inactivation that occurs during each depolarization is likely to be mechanistically distinct from the late phase of slow inactivation blocked by mutations N49K and R3C. Our results are consistent with the model that R3 must move outward through the gating pore and engage Asn49 to trigger the late, slowly reversible slow-inactivation process of NavAb.

Mutations N49K and R3C each produce ∼75–102-mV positive shifts in the voltage dependence of activation, indicating that they greatly stabilize the resting state of the voltage sensor relative to its activated state. Mutation R4C produces a large (∼43-mV) positive shift in the voltage dependence of activation, suggesting that it too greatly stabilizes the resting state relative to the activated state. The simplest interpretation of these data is that an interaction between R3 and Asn49 is required for normal voltage-dependent activation of NavAb and for coupling to the late absorbing form of slow inactivation. Conversely, because the mutation NavAb/R4C does not block late slow inactivation, interactions of R4 are not necessary for this inactivation process. R4 can interact with the Asn49 equivalent, D60, in NaChBac in the activated voltage sensor (DeCaen et al., 2008, 2009). Our finding that the NavAb/R3C does not enter the late slow-inactivated state, despite the presence of R4, suggests that R4 interaction with Asn49 is not sufficient to induce late slow inactivation on its own and therefore is neither necessary nor sufficient to induce the late slow-inactivated state.

Interactions of R3 with Asn49 in crystal structures of NavAb

The crystal structure of the preopen state of NavAb shows that Asn49 is positioned close to R2 and R3 on the extracellular side of the hydrophobic constriction site in an activated state of the voltage sensor. At an estimated distance of 3.6–3.9 Å, the interaction of R3 with Asn49 is weaker than the interaction of R3 with other interacting partners, but it is close enough to have a small effect to stabilize the activated state of the voltage sensor captured in the crystal (Payandeh et al., 2011). However, at least in this preopen state, the available crystal structure does not provide a basis for interpretation of the full effect of mutation N49K on the voltage dependence of activation in terms of destabilization of the activated voltage sensor by breaking interaction of R3 with Asn49. On the other hand, substitution of the large positively charged Lys residue in this position would create charge–charge repulsion between R3 and Lys49 that would destabilize the activated state.

In the lower resolution structures of NavAb WT in two potentially slow-inactivated states (Payandeh et al., 2012), R3 is closer to Asn49 at 3.3–3.5 Å and appears to make an energetically significant interaction in these states. Although more high resolution structures are needed, the current structures raise the possibility that new interactions between R3 and Asn49 may form in slow-inactivated states and may contribute to the driving force for the inactivation process. These structures of

NavAb WT are thought to represent a slow-inactivated state because of the asymmetric collapse of the selectivity filter, internal cavity, and activation gate. Mutating a neutral amino acid (Asn49) to a positively charged one (Lys) would lead to loss of favorable electrostatic interactions and induce repulsive interactions between the R3 gating charge and Asn49, which could contribute to the impairment of slow inactivation by mutation of this residue. In the same structures of NavAb (Payandeh et al., 2011, 2012), the Cα of R4 is positioned at the intracellular edge of the hydrophobic constriction site, and its side chain interacts with the intracellular negatively charged cluster. Thus, these structural results agree with our functional studies showing that R4 interaction with Asn49 is not required for slow inactivation.

Comparison to gating charge interactions during activation and inactivation of NaChBac

Interactions of R3 and R4 with the N49 equivalent (Asp60) have been studied in NaChBac by disulfide cross-linking (DeCaen et al., 2008, 2009). R3C cross-links spontaneously with D60C upon depolarization, and R4C cross-links spontaneously with E70C, enforcing conformations of the voltage sensor that are similar to those seen in the NavAb crystal structure. R4C also forms cross-links to D60C, but cross-linking was slower and required an oxidizing reagent. This cross-link presumably stabilizes the voltage sensor in a more outward, activated conformation. In NaChBac, each of these three molecular cross-links led to activation followed by entry into a slow-inactivated state, and all three cross-links likely lock interaction of R3 with D60. Thus, the observation of slow inactivation in each of these constructs is consistent with interaction between the residues at the positions of R3 and D60 in the slow-inactivated state of NaChBac (Payandeh et al., 2012). Inactivation after the slower oxidation-induced cross-linking of NaChBac/D60C-R4C suggests that this molecular interaction can also support the slow-inactivation process. It is possible that this further outward movement of the S4 segment produces a more stable form of slow inactivation in NaChBac (DeCaen et al., 2008, 2009).

Coupling between slow inactivation and gating charge hysteresis

We found that the N49K mutation does not abolish hysteresis of charge movement in response to depolarization. Gating charge hysteresis is induced by prolonged depolarization in multiple types of ion channels and has been correlated with slow inactivation (Bezanilla et al., 1982; Brum and Rios, 1987; Olcese et al., 1996, 1997). It also occurs in the isolated voltage-sensing domains of Ci-VSP channels (Villalba-Galea et al., 2008, 2009), and it is retained in noninactivating mutants of hERG channels (Tristani-Firouzi et al., 2002; Piper et al., 2003) and in HCN channels (Männikkö et al., 2005) that do not undergo slow inactivation. More recently, it has been proposed that intrinsic hysteresis of the voltage-sensor domain in Shaker potassium channels, and perhaps other voltage-gated channels, is caused by the mechanical load imparted by the pore (Haddad and Blunck, 2011), and long molecular dynamics simulations indicate that the pore closes before the inward movement of most of the gating charge, as expected from this model (Jensen et al., 2012). Thus, hysteresis and slow inactivation are not necessarily linked, although they may influence each other allosterically and energetically. Our findings are consistent with this general theme in that hysteresis is induced by depolarizations that cause slow inactivation, but hysteresis is maintained in N49K, even though slow inactivation is abolished.

Multiple forms of inactivation in eukaryotic sodium channels

Slow inactivation of eukaryotic sodium channels occurs with complex kinetics and has been linked to many structural parts of the channel by site-directed mutagenesis (Vilin and Ruben, 2001; Ulbricht, 2005), but few studies have implicated the voltage sensors directly in slow inactivation. Modification of R3C by negatively charged methanethiosulfonate-ethylsulfate in the voltage sensor of domain IV of $Na_V1.4$ enhances slow inactivation (Mitrovic et al., 2000), suggesting the involvement of this voltage sensor in slow inactivation. Prolonged depolarizations that induce slow inactivation stabilize an activated conformation of the domain IV voltage sensor of $Na_V1.4$ (Cha et al., 1999; Capes et al., 2012). The outer mouth of the ion-conducting pore has been implicated in slow inactivation in many studies (Capes et al., 2012), and the pore-blocking toxin, tetrodotoxin, also stabilizes the activated conformation of the domain IV voltage sensor (Capes et al., 2012). These results on mammalian sodium channels are consistent with the link between the voltage-sensing domain and the slow-inactivation process implied by our results.

N49-equivalent substitutions in voltage-gated potassium channels

The equivalent position of N49 in the Shaker potassium channel is E283. It interacts with gating charges R2 and R3 in the crystal structure of the voltage sensor of $K_V1.2$ channels (Long et al., 2005), which closely resembles NavAb in conformation (Payandeh et al., 2011). Neutralization of E283 and equivalent residues shifts the voltage dependence of activation dramatically to more positive potentials, which illustrates the role of these residues in stabilizing the resting state of the voltage sensor relative to its activated state in potassium channels (Papazian et al., 1995; Planells-Cases et al., 1995; Pless et al., 2011), as we have observed in NavAb. Attempts to reverse the charge of E283-equivalent residues led to nonfunctional channels (Tiwari-Woodruff et al., 1997; Wu et al., 2010). NavAb is unusual among homotetrameric ion channels in having a neutral amino acid at this position (Payandeh et al., 2011), and both NaChBac and NavAb are unusual in tolerating

substitution of a positive charge at this position (this paper and Zhao et al., 2004b).

Potassium channels also inactivate by conformational changes in the pore (Bähring et al., 2012), and the non–voltage-gated potassium channel KcsA enters a series of inactivated states with increasing degrees of collapse of the selectivity filter and pore that have been captured in crystal structures (Cuello et al., 2010a,b). These inactivated states have a general similarity to the asymmetric collapse of the pore observed in inactivated NavAb and a distantly related bacterial Nav channel (Payandeh et al., 2012; Zhang et al., 2012). The clearest functional definition of the inactivated states of voltage-gated potassium channels suggests a stepwise transition to a P-type–inactivated state that involves conformational changes in the selectivity filter, and then to a more stable C-type–inactivated state that involves conformational changes in the pore-lining S6 segment. Only the latter C-type transition is associated with voltage-sensor hysteresis (De Biasi et al., 1993; Olcese et al., 1997; Yang et al., 1997; Loots and Isacoff, 1998). One scenario suggests that C-type inactivation is always preceded by P-type inactivation that involves a reorientation of some residues in the selectivity filter. This conformational change is transmitted to the S6 segment, leading to C-type inactivation. The molecular forces that drive the selectivity filter into its collapsed conformation are not well understood, but a collapsed state of the pore is a key feature in molecular dynamics simulations of $K_V1.2$ channel gating (Jensen et al., 2010, 2012).

The S4 voltage sensor plays a critical role in controlling the inactivation process of *Shaker* potassium channels. Residues in the pore sense voltage-sensor conformation, and rearrangements in the pore domain are triggered and stabilized by interaction with the voltage sensor S4 (Loots and Isacoff, 1998). It appears that the S4 segment interacts with the pore domain electrostatically (Loots and Isacoff, 2000; Lainé et al., 2003; Soler-Llavina et al., 2006), where the uppermost arginine residue (from the N-terminal side) has an atomic proximity to residues located in the P-domain. This proximity was manifested by disulfide locking of R1C in S4 with F416C and A419C in the P-region (Lainé et al., 2003). Interactions like these could underlie the late slow inactivation of WT Na_VAb, and blocking the interaction of N49 and R3 could prevent conformational changes that normally lead to such interactions and late slow inactivation.

Research reported in this publication was supported by the National Institute of Neurological Disorders and Stroke (NINDS) of the National Institutes of Health (NIH) under award number R01NS015751, and the National Heart, Lung, and Blood Institute (NHLBI) of the NIH under award number R01HL112808. The content is solely the responsibility of the authors and does not necessarily represent the official views of the NIH.

Kenton J. Swartz served as editor.

Submitted: 19 April 2013
Accepted: 1 August 2013

REFERENCES

Bähring, R., J. Barghaan, R. Westermeier, and J. Wollberg. 2012. Voltage sensor inactivation in potassium channels. *Front Pharmacol.* 3:100. http://dx.doi.org/10.3389/fphar.2012.00100

Bezanilla, F., R.E. Taylor, and J.M. Fernández. 1982. Distribution and kinetics of membrane dielectric polarization. 1. Long-term inactivation of gating currents. *J. Gen. Physiol.* 79:21–40. http://dx.doi.org/10.1085/jgp.79.1.21

Blanchet, J., S. Pilote, and M. Chahine. 2007. Acidic residues on the voltage-sensor domain determine the activation of the NaChBac sodium channel. *Biophys. J.* 92:3513–3523. http://dx.doi.org/10.1529/biophysj.106.090464

Brum, G., and E. Rios. 1987. Intramembrane charge movement in frog skeletal muscle fibres. Properties of charge 2. *J. Physiol.* 387:489–517.

Capes, D.L., M. Arcisio-Miranda, B.W. Jarecki, R.J. French, and B. Chanda. 2012. Gating transitions in the selectivity filter region of a sodium channel are coupled to the domain IV voltage sensor. *Proc. Natl. Acad. Sci. USA.* 109:2648–2653. http://dx.doi.org/10.1073/pnas.1115575109

Catterall, W.A. 2000. From ionic currents to molecular mechanisms: the structure and function of voltage-gated sodium channels. *Neuron.* 26:13–25. http://dx.doi.org/10.1016/S0896-6273(00)81133-2

Cha, A., P.C. Ruben, A.L. George Jr., E. Fujimoto, and F. Bezanilla. 1999. Voltage sensors in domains III and IV, but not I and II, are immobilized by Na^+ channel fast inactivation. *Neuron.* 22:73–87. http://dx.doi.org/10.1016/S0896-6273(00)80680-7

Chen, L.Q., V. Santarelli, R. Horn, and R.G. Kallen. 1996. A unique role for the S4 segment of domain 4 in the inactivation of sodium channels. *J. Gen. Physiol.* 108:549–556. http://dx.doi.org/10.1085/jgp.108.6.549

Chen, Y., F.H. Yu, D.J. Surmeier, T. Scheuer, and W.A. Catterall. 2006. Neuromodulation of Na^+ channel slow inactivation via cAMP-dependent protein kinase and protein kinase C. *Neuron.* 49:409–420. http://dx.doi.org/10.1016/j.neuron.2006.01.009

Cuello, L.G., V. Jogini, D.M. Cortes, A.C. Pan, D.G. Gagnon, O. Dalmas, J.F. Cordero-Morales, S. Chakrapani, B. Roux, and E. Perozo. 2010a. Structural basis for the coupling between activation and inactivation gates in K^+ channels. *Nature.* 466:272–275. http://dx.doi.org/10.1038/nature09136

Cuello, L.G., V. Jogini, D.M. Cortes, and E. Perozo. 2010b. Structural mechanism of C-type inactivation in K^+ channels. *Nature.* 466:203–208. http://dx.doi.org/10.1038/nature09153

De Biasi, M., H.A. Hartmann, J.A. Drewe, M. Taglialatela, A.M. Brown, and G.E. Kirsch. 1993. Inactivation determined by a single site in K^+ pores. *Pflugers Arch.* 422:354–363. http://dx.doi.org/10.1007/BF00374291

DeCaen, P.G., V. Yarov-Yarovoy, Y. Zhao, T. Scheuer, and W.A. Catterall. 2008. Disulfide locking a sodium channel voltage sensor reveals ion pair formation during activation. *Proc. Natl. Acad. Sci. USA.* 105:15142–15147. http://dx.doi.org/10.1073/pnas.0806486105

DeCaen, P.G., V. Yarov-Yarovoy, E.M. Sharp, T. Scheuer, and W.A. Catterall. 2009. Sequential formation of ion pairs during activation of a sodium channel voltage sensor. *Proc. Natl. Acad. Sci. USA.* 106:22498–22503. http://dx.doi.org/10.1073/pnas.0912307106

Haddad, G.A., and R. Blunck. 2011. Mode shift of the voltage sensors in Shaker K^+ channels is caused by energetic coupling to the pore domain. *J. Gen. Physiol.* 137:455–472. http://dx.doi.org/10.1085/jgp.201010573

Hodgkin, A.L., and A.F. Huxley. 1952. A quantitative description of membrane current and its application to conduction and excitation in nerve. *J. Physiol.* 117:500–544.

Jensen, M.Ø., D.W. Borhani, K. Lindorff-Larsen, P. Maragakis, V. Jogini, M.P. Eastwood, R.O. Dror, and D.E. Shaw. 2010. Principles

of conduction and hydrophobic gating in K^+ channels. *Proc. Natl. Acad. Sci. USA.* 107:5833–5838. http://dx.doi.org/10.1073/pnas.0911691107

Jensen, M.Ø., V. Jogini, D.W. Borhani, A.E. Leffler, R.O. Dror, and D.E. Shaw. 2012. Mechanism of voltage gating in potassium channels. *Science.* 336:229–233. http://dx.doi.org/10.1126/science.1216533

Kühn, F.J., and N.G. Greeff. 1999. Movement of voltage sensor S4 in domain 4 is tightly coupled to sodium channel fast inactivation and gating charge immobilization. *J. Gen. Physiol.* 114:167–183. http://dx.doi.org/10.1085/jgp.114.2.167

Lainé, M., M.C. Lin, J.P. Bannister, W.R. Silverman, A.F. Mock, B. Roux, and D.M. Papazian. 2003. Atomic proximity between S4 segment and pore domain in Shaker potassium channels. *Neuron.* 39:467–481. http://dx.doi.org/10.1016/S0896-6273(03)00468-9

Long, S.B., E.B. Campbell, and R. Mackinnon. 2005. Crystal structure of a mammalian voltage-dependent Shaker family K^+ channel. *Science.* 309:897–903. http://dx.doi.org/10.1126/science.1116269

Loots, E., and E.Y. Isacoff. 1998. Protein rearrangements underlying slow inactivation of the Shaker K^+ channel. *J. Gen. Physiol.* 112:377–389. http://dx.doi.org/10.1085/jgp.112.4.377

Loots, E., and E.Y. Isacoff. 2000. Molecular coupling of S4 to a K^+ channel's slow inactivation gate. *J. Gen. Physiol.* 116:623–636. http://dx.doi.org/10.1085/jgp.116.5.623

Männikkö, R., S. Pandey, H.P. Larsson, and F. Elinder. 2005. Hysteresis in the voltage dependence of HCN channels: Conversion between two modes affects pacemaker properties. *J. Gen. Physiol.* 125:305–326. http://dx.doi.org/10.1085/jgp.200409130

Mitrovic, N., A.L. George Jr., and R. Horn. 2000. Role of domain 4 in sodium channel slow inactivation. *J. Gen. Physiol.* 115:707–718. http://dx.doi.org/10.1085/jgp.115.6.707

Olcese, R., A. Neely, N. Qin, X. Wei, L. Birnbaumer, and E. Stefani. 1996. Coupling between charge movement and pore opening in vertebrate neuronal alpha 1E calcium channels. *J. Physiol.* 497:675–686.

Olcese, R., R. Latorre, L. Toro, F. Bezanilla, and E. Stefani. 1997. Correlation between charge movement and ionic current during slow inactivation in Shaker K^+ channels. *J. Gen. Physiol.* 110:579–589. http://dx.doi.org/10.1085/jgp.110.5.579

Papazian, D.M., X.M. Shao, S.A. Seoh, A.F. Mock, Y. Huang, and D.H. Wainstock. 1995. Electrostatic interactions of S4 voltage sensor in Shaker K^+ channel. *Neuron.* 14:1293–1301. http://dx.doi.org/10.1016/0896-6273(95)90276-7

Pavlov, E., C. Bladen, R. Winkfein, C. Diao, P. Dhaliwal, and R.J. French. 2005. The pore, not cytoplasmic domains, underlies inactivation in a prokaryotic sodium channel. *Biophys. J.* 89:232–242. http://dx.doi.org/10.1529/biophysj.104.056994

Payandeh, J., T. Scheuer, N. Zheng, and W.A. Catterall. 2011. The crystal structure of a voltage-gated sodium channel. *Nature.* 475:353–358. http://dx.doi.org/10.1038/nature10238

Payandeh, J., T.M. Gamal El-Din, T. Scheuer, N. Zheng, and W.A. Catterall. 2012. Crystal structure of a voltage-gated sodium channel in two potentially inactivated states. *Nature.* 486:135–139.

Piper, D.R., A. Varghese, M.C. Sanguinetti, and M. Tristani-Firouzi. 2003. Gating currents associated with intramembrane charge displacement in HERG potassium channels. *Proc. Natl. Acad. Sci. USA.* 100:10534–10539. http://dx.doi.org/10.1073/pnas.1832721100

Planells-Cases, R., A.V. Ferrer-Montiel, C.D. Patten, and M. Montal. 1995. Mutation of conserved negatively charged residues in the S2 and S3 transmembrane segments of a mammalian K^+ channel selectively modulates channel gating. *Proc. Natl. Acad. Sci. USA.* 92:9422–9426. http://dx.doi.org/10.1073/pnas.92.20.9422

Pless, S.A., J.D. Galpin, A.P. Niciforovic, and C.A. Ahern. 2011. Contributions of counter-charge in a potassium channel voltage-sensor domain. *Nat. Chem. Biol.* 7:617–623. http://dx.doi.org/10.1038/nchembio.622

Ren, D., B. Navarro, H. Xu, L. Yue, Q. Shi, and D.E. Clapham. 2001. A prokaryotic voltage-gated sodium channel. *Science.* 294:2372–2375. http://dx.doi.org/10.1126/science.1065635

Ruben, P.C., J.G. Starkus, and M.D. Rayner. 1990. Holding potential affects the apparent voltage-sensitivity of sodium channel activation in crayfish giant axons. *Biophys. J.* 58:1169–1181. http://dx.doi.org/10.1016/S0006-3495(90)82458-9

Rudy, B. 1978. Slow inactivation of the sodium conductance in squid giant axons. Pronase resistance. *J. Physiol.* 283:1–21.

Ruff, R.L., L. Simoncini, and W. Stühmer. 1987. Comparison between slow sodium channel inactivation in rat slow- and fast-twitch muscle. *J. Physiol.* 383:339–348.

Soler-Llavina, G.J., T.H. Chang, and K.J. Swartz. 2006. Functional interactions at the interface between voltage-sensing and pore domains in the Shaker K_v channel. *Neuron.* 52:623–634. http://dx.doi.org/10.1016/j.neuron.2006.10.005

Tiwari-Woodruff, S.K., C.T. Schulteis, A.F. Mock, and D.M. Papazian. 1997. Electrostatic interactions between transmembrane segments mediate folding of Shaker K^+ channel subunits. *Biophys. J.* 72:1489–1500. http://dx.doi.org/10.1016/S0006-3495(97)78797-6

Tristani-Firouzi, M., J. Chen, and M.C. Sanguinetti. 2002. Interactions between S4-S5 linker and S6 transmembrane domain modulate gating of HERG K^+ channels. *J. Biol. Chem.* 277:18994–19000. http://dx.doi.org/10.1074/jbc.M200410200

Ulbricht, W. 2005. Sodium channel inactivation: molecular determinants and modulation. *Physiol. Rev.* 85:1271–1301. http://dx.doi.org/10.1152/physrev.00024.2004

Vassilev, P.M., T. Scheuer, and W.A. Catterall. 1988. Identification of an intracellular peptide segment involved in sodium channel inactivation. *Science.* 241:1658–1661. http://dx.doi.org/10.1126/science.2458625

Vilin, Y.Y., and P.C. Ruben. 2001. Slow inactivation in voltage-gated sodium channels: molecular substrates and contributions to channelopathies. *Cell Biochem. Biophys.* 35:171–190. http://dx.doi.org/10.1385/CBB:35:2:171

Vilin, Y.Y., E. Fujimoto, and P.C. Ruben. 2001. A single residue differentiates between human cardiac and skeletal muscle Na^+ channel slow inactivation. *Biophys. J.* 80:2221–2230. http://dx.doi.org/10.1016/S0006-3495(01)76195-4

Villalba-Galea, C.A., W. Sandtner, D.M. Starace, and F. Bezanilla. 2008. S4-based voltage sensors have three major conformations. *Proc. Natl. Acad. Sci. USA.* 105:17600–17607. http://dx.doi.org/10.1073/pnas.0807387105

Villalba-Galea, C.A., W. Sandtner, D. Dimitrov, H. Mutoh, T. Knöpfel, and F. Bezanilla. 2009. Charge movement of a voltage-sensitive fluorescent protein. *Biophys. J.* 96:L19–L21. http://dx.doi.org/10.1016/j.bpj.2008.11.003

Wu, D., K. Delaloye, M.A. Zaydman, A. Nekouzadeh, Y. Rudy, and J. Cui. 2010. State-dependent electrostatic interactions of S4 arginines with E1 in S2 during Kv7.1 activation. *J. Gen. Physiol.* 135:595–606. http://dx.doi.org/10.1085/jgp.201010408

Yang, Y., Y. Yan, and F.J. Sigworth. 1997. How does the W434F mutation block current in Shaker potassium channels? *J. Gen. Physiol.* 109:779–789. http://dx.doi.org/10.1085/jgp.109.6.779

Zhang, X., W. Ren, P. DeCaen, C. Yan, X. Tao, L. Tang, J. Wang, K. Hasegawa, T. Kumasaka, J. He, et al. 2012. Crystal structure of an orthologue of the NaChBac voltage-gated sodium channel. *Nature.* 486:130–134. http://dx.doi.org/10.1038/nature11054

Zhao, Y., T. Scheuer, and W.A. Catterall. 2004a. Reversed voltage-dependent gating of a bacterial sodium channel with proline substitutions in the S6 transmembrane segment. *Proc. Natl. Acad. Sci. USA.* 101:17873–17878. http://dx.doi.org/10.1073/pnas.0408270101

Zhao, Y., V. Yarov-Yarovoy, T. Scheuer, and W.A. Catterall. 2004b. A gating hinge in Na^+ channels: a molecular switch for electrical signaling. *Neuron.* 41:859–865. http://dx.doi.org/10.1016/S0896-6273(04)00116-3